Marc Martí-Sabaté, Sébastien Guenneau and Dani Torrent

View Online   Export Citation   CrossMark

ARTICLES YOU MAY BE INTERESTED IN

Single and coupled Helmholtz resonators for low frequency sound manipulation
Journal of Applied Physics **132**, 064505 (2022); https://doi.org/10.1063/5.0096630

The effect of organic coatings in the magnetization of $CoFe_2O_4$ nanoparticles
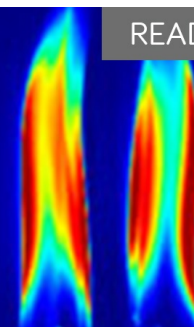AIP Advances **12**, 085102 (2022); https://doi.org/10.1063/5.0078167

Correct use of excess configurational entropies to study the ideal glass transition in hard-sphere systems with continuous polydispersity
AIP Advances **12**, 085204 (2022); https://doi.org/10.1063/5.0096421

AIP Advances

Fluids and Plasmas Collection

READ NOW

High-quality resonances in quasi-periodic clusters of scatterers for flexural waves

View Online   Export Citation   CrossMark

Marc Martí-Sabaté,[1] (iD) Sébastien Guenneau,[2] and Dani Torrent[1,a] (iD)

AFFILIATIONS

[1] GROC, UJI, Institut de Noves Tecnologies de la Imatge (INIT), Universitat Jaume I, 12071 Castelló, Spain
[2] UMI 2004 Abraham de Moivre-CNRS, Imperial College London, London SW7 2AZ, United Kingdom

[a] Author to whom correspondence should be addressed: dtorrent@uji.es

ABSTRACT

Multiple scattering theory is applied to the study of clusters of point-like scatterers attached to a thin elastic plate and arranged in quasi-periodic distributions. Two types of structures are specifically considered: the twisted bilayer and the quasi-periodic line. The former consists in a couple of two-dimensional lattices rotated a relative angle, so that the cluster forms a moiré pattern. The latter can be seen as a periodic one-dimensional lattice where an incommensurate modulation is superimposed. Multiple scattering theory allows for the fast and efficient calculation of the resonant modes of these structures as well as for their quality factor, which is thoroughly analyzed in this work. The results show that quasi-periodic structures present a large density of states with high quality factors, being therefore a promising way for the design of high quality wave-localization devices.

I. INTRODUCTION

The study of quasi-periodic structures has a long history in all domains of physics,[1–8] although recently an increasing interest has emerged due to the extraordinary properties of twisted bilayer graphene.[9–11]

In the realm of classical waves (mainly photonic and acoustics), different quasi-periodic structures have been recently studied in one and two dimensions, and localized and robust interface states have been found both theoretically and experimentally.[12–20] The theoretical analysis of quasi-periodic distributions of scatterers is extremely challenging, since these contain a large number of scatterers and some periodicity might only be retrieved in a higher-dimensional space, where the analysis might be simplified making use of a single unit cell.[21] Recently, we found that multiple scattering theory is a reliable method for the study of quasi-periodic arrangement of scatterers,[22,23] and we showed that these structures present a large density of states.

However, the analysis of these states is incomplete if the imaginary part of the frequency is not taken into account, since open systems have finite mean-life resonances whose quality can be more than relevant for their use as wave-trapping devices. Consequently, a deeper analysis of these structures has yet to be done.

In this work, we will revisit the structures studied in Refs. 22 and 23 to further analyze the resonances found therein. Multiple scattering theory allows for the analysis of the resonances' quality in finite clusters of scatterers. This can be done mainly by two methods, based on the analysis of the response of the system to real or complex frequencies. Both methods are similar for high quality resonances, but only the latter is accurate for low quality factor resonances, as will be shown in the following sections.

This paper is organized as follows: After this introduction, in Sec. II, we will present a brief description of the use of multiple scattering theory for the analysis of resonant frequencies of finite clusters of scatterers. Then, Sec. III will analyze the quality factor of the eigenmodes of the quasi-periodic line of scatterers, and in Sec. IV, the same analysis will be performed for the two-dimensional twisted bilayer structure. Finally, Sec. V will summarize the work.

II. RESONANT MODES BY MULTIPLE SCATTERING THEORY

Given a cluster of N point scatterers attached to a thin elastic plate at positions $\boldsymbol{R}_\alpha$, for $\alpha = 1, \ldots, N$, the eigenmodes of such a cluster are defined as the zeros of the determinant of the

multiple scattering matrix M when no incident field is present.[22,23] This matrix is defined as

$$M_{\alpha\beta} = \delta_{\alpha\beta} t_\alpha^{-1} - G(\mathbf{R}_\alpha - \mathbf{R}_\beta), \qquad (1)$$

where Green's function $G(\boldsymbol{r})$ for flexural waves is given by

$$G(\boldsymbol{r}) = \frac{i}{8k^2}[H_0(kr) - H_0(ikr)], \qquad (2)$$

and the scalar quantity t_α defines the impedance of each scatterer.[22–26]

The matrix M is a function of frequency via both t_α and $G(\boldsymbol{r})$. However, the determinant is never zero for a real frequency for an open system (spectra of open systems depart from the real line and populate the complex plane[27]), as it is the case of our finite cluster. Therefore, in order to find the eigenmodes of the cluster, we should solve the equation

$$\det M(\Omega) = 0 \qquad (3)$$

for a complex frequency ω. The real part of such a complex frequency corresponds to the peak expected upon excitation of the cluster while the imaginary part is related with the quality factor of the eigenmode, i.e., the larger the imaginary part, the lower the quality factor.

Finding the complex zeros of a determinant is in general a difficult problem, since the determinant itself is complex-valued. However, an approximate value for the real part of the eigenfrequency can be obtained as those frequencies that minimize the value of the determinant, or, more efficiently, those frequencies that minimize the smallest eigenvalue of the matrix M. If the quality of the resonance is high, it will have a small imaginary part so that the complex zero can be found around the approximate real frequency that minimizes the smallest eigenvalue of M. Obviously, the closer the smallest eigenvalue to zero, the smaller the imaginary part of the eigenfrequency.

If the analysis is performed only analyzing the behavior of the minimum eigenvalue as a function of the real part of the frequency, the quality factor can be found from the response in the neighborhood of the minimum. Thus, the quality factor of a resonance is defined as

$$Q = \frac{f_0}{\delta f}, \qquad (4)$$

with f_0 being the resonant frequency and δf the full width half maximum.

Both methods will be applied below for the characterization of the eigenmodes of the clusters.

III. ONE-DIMENSIONAL ARRAY OF SCATTERERS

We will consider first the analysis of eigenfrequencies of one-dimensional arrays of scatterers. Let us assume that a cluster of N scatterers are arranged in positions $\mathbf{R}_\alpha$ as shown in Fig. 1, lower panel, such that

$$\mathbf{R}_\alpha = a\alpha + \rho_m \sin(\alpha\theta), \qquad (5)$$

with a being the lattice constant, ρ_m the radius of the modulation circle, and θ the angle rotated in the circle (as defined
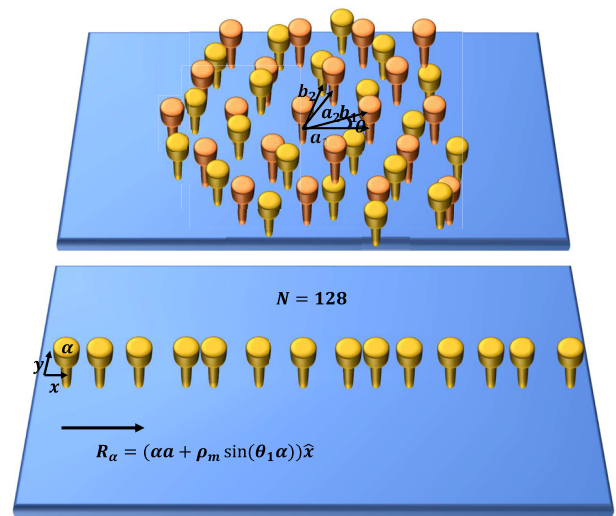

FIG. 1. Schematics of the two structures analyzed in this work: A twisted bilayer configuration (upper panel) and an aperiodic line of scatterers (lower panel). The scatterers consist of spring-mass resonators attached to a thin elastic plate by means of a point-like contact. The geometrical parameters are indicated in the drawing (see text for further explanation).

in Ref. 28). This type of arrangement allows us to define periodic or aperiodic clusters depending on the nature of the θ parameter (rational or irrational, respectively).

Figure 2, left panel, shows the evolution of the minimum eigenvalue of the M matrix as a function of the normalized frequency of the system (only real component) and the modulation parameter θ. The diagram shows the well-known Hofstadter's butterfly,[29] and it was previously found for these systems.[23] This structure is
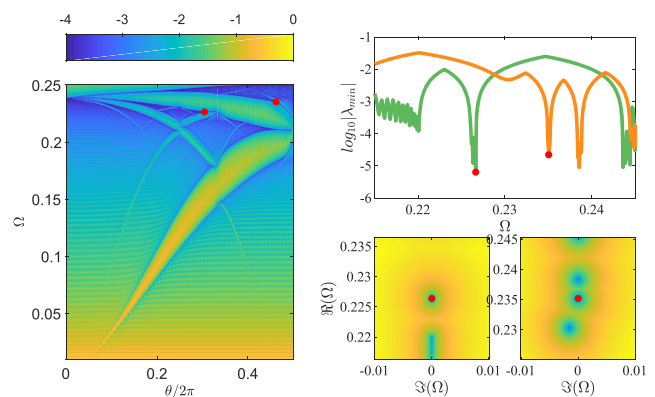

FIG. 2. Left panel: evolution of the minimum eigenvalue of the multiple scattering matrix (M) as a function of the modulation parameter of a one-dimensional array of scatterers and the normalized frequency of the system (real frequency). The scatterers' properties are $\gamma_\alpha = 100$ and $\Omega_\alpha \cdot a/\pi = 0.25$. Upper right panel: evolution of the minimum eigenvalue as a function of the normalized frequency for two spatial configurations, corresponding to $\theta = 0.26°$ and $\theta = 0.45°$. Lower right panels: these two maps show the evolution of the minimum eigenvalue as a function of the normalized frequency of the system in the complex plane.

characterized by a set of gaps without modes all over the spectrum, defining the contour of the butterfly (yellow and green regions in Fig. 2 left panel). The upper right panel of Fig. 2 shows the frequency evolution of the smallest eigenvalue for $\theta = 0.26°$ (green line) and $\theta = 0.45°$ (orange line). Two points, highlighted in red, belong to two different zones where two bandgaps are approaching each other. These bandgaps will collapse as the modulation parameter increases; however, before this occurs, they confine a state in between. The green line shows a resonance in the middle of two bandgaps, and at low frequencies, several resonances appear. The complex frequency map shown below also depicts these minima: the imaginary part that must be added in order to obtain the cancellation of the eigenvalue is negligible. Concerning the second configuration, one minimum has been chosen (red point). However, the chosen window lets us appreciate four different minima in the eigenvalue; three of them having high quality factor, while another one having low quality factor (near $\Omega = 0.23$). The complex frequency map below also shows these four minima: the three in the upper part correspond to the high quality resonances; they are at the center of the map, with almost null imaginary frequency component. Meanwhile, the fourth resonance is shifted to the left, stating the need of a higher imaginary component for achieving the cancellation of the determinant.

These modes tend to localize at the edge of the structure, so that by adding the mirror symmetric cluster we will increase the robustness of the mode, as will be shown below. They appear as a consequence of having a finite structure. If we were able to simulate the infinite structure, we would not be able to find these modes inside the gap. This result can be approached by only evaluating our structure for modulation parameters such that

$$\theta = \frac{n}{N}, \quad n = 1, \ldots, N, \tag{6}$$

with N being the number of scatterers in the finite cluster, as explained in Ref. 30. Edge states became interface states by the addition of mirror symmetry.

Figure 3, upper panels, show the same insight of the Hofstadter butterfly, but the left map corresponds to the linear array of scatterers without mirror symmetry, while the second one corresponds to the addition of mirror symmetry to the structure. These insights are centered in a bandgap; therefore, the vertical lines that appear in both maps (in the left one they are hardly visible, while they are clearer in the right one) correspond to modes inside the gap. One point has been chosen from each map (they have not exactly the same properties due to the fact that vertical lines are slightly shifted when adding the mirror symmetry to the structure). Figure 3 lower panel shows the evolution of the eigenvalue as a function of the normalized frequency for the spatial configuration of the red points. Whereas the simple structure shows a low quality factor resonance with a minimum far from zero, the mirror-symmetric structure presents a narrower resonance (high quality factor) and the minimum is two orders of magnitude smaller than the former one.

Figure 4 shows another example of the improvement in the bandgap modes due to the addition of symmetry. In this case, the chosen spatial configuration is found inside one of the smaller bandgaps of the Hofstadter's butterfly. However, the result is similar: the evolution of the eigenvalue as a function of the frequency shows that the resonance inside the bandgap gets narrower when adding spatial symmetry to the system.
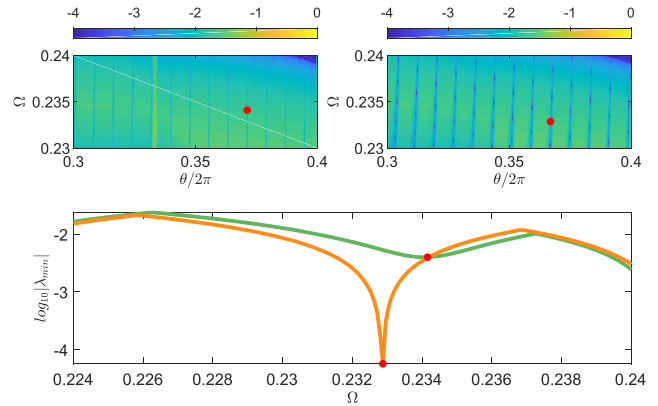

FIG. 3. Resonance comparison between modes found in the gaps of the Hofstadter's butterfly for a one-dimensional array of scatterers (upper left panel) and bandgap modes found for a one-dimensional array of scatterers with mirror symmetry (upper right pannel). Lower panel: evolution of the minimum eigenvalue as a function of the normalized frequency for both structures with a given spatial configuration. As can be seen, the mirror-symmetric structure presents a sharper resonance compared with the simpler structure.

As discussed before, we expect a small imaginary part for these two resonances when the zeros are searched in the complex plane, since the eigenvalue is very close to zero.

IV. TWISTED BILAYERS

In this section, we will perform a similar analysis but for the twisted bilayer analyzed in Ref. 22. This analysis is motivated by the fractal energy landscapes of twisted bilayers,[31] similarly to the Hofstadter butterfly spectrum of the finite cluster studied previously. We will build clusters of scatterers by the superposition of two identical periodic lattices with a relative angle between their lattice vectors. Thus, defining the first lattice vectors as $\mathbf{a_l} = a_{lx} + i a_{ly}$,
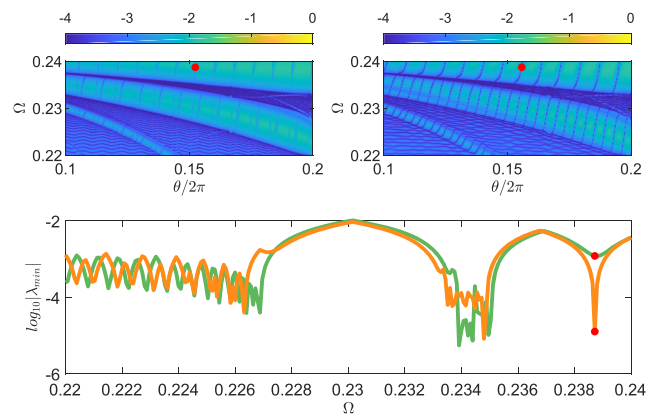

FIG. 4. Another example of comparison between one-dimensional arrays of scatterers (upper left panel) and one-dimensional arrays of scatterers with mirror symmetry (upper right panel). Again, the lower panel shows the evolution of the minimum eigenvalue for a given spatial configuration, showing that the resonance near $\Omega = 0.24$ is sharper in the case of the mirror-symmetric structure.

for $l = 1, 2$, and similarly for the second lattice ($\mathbf{b_l} = b_{lx} + ib_{ly}$), they will be simply related as $\mathbf{b_l} = \mathbf{a_l} e^{i\theta_0}$, being θ_0 the twisting angle between both lattices. Scatterers in the cluster are located at positions $R_a = n_1\mathbf{a_1} + n_2\mathbf{a_2}$ and $R_b = m_1\mathbf{b_1} + m_2\mathbf{b_2}$, being n_i, m_i integer numbers.

Figure 5, left panel, shows the evolution of the minimum eigenvalue of the M matrix as a function of the normalized frequency of the system and the twisting angle of the bilayer structure. Blue lines in the map correspond to configurations where the eigenvalue approaches zero. The individual lattices forming the twisted bilayer have triangular arrangement, and the properties of the scatterers are constant ($\Omega_\alpha a/\pi = 20$ and $\gamma_\alpha = 200$). Triangular lattices have $\pi/6$ symmetry; therefore, only the twisting angles between $0°$ and $30°$ have been shown. As explained in Ref. 22, modes are located around commensurate angles of the twisted bilayer and also near small twisting angles. Two points have been chosen in the map: they have been highlighted in red. In the upper right panel, the evolution of the minimum eigenvalue with frequency is shown for the two spatial configurations of the highlighted points: they correspond to $\theta = 9.1°$ and $\theta = 9.3°$. Both curves present a resonance, being the red point the minimum of the resonance. However, while the first curve shows a sharp resonance with a high quality factor ($Q = 81.4$), the second curve has a broader resonance with low quality factor ($Q = 4.6$).

As explained before, once the resonant frequency has been found, a detailed analysis in the complex frequency plane can be done. Figure 5 lower panels show the evolution of the minimum eigenvalue as a function of the complex normalized frequency of the system. Both maps are centered at the resonant frequencies of the chosen modes (red points). The first case, which presented a sharp resonance, shows the minimum in the center of the complex map, with a slight shift with respect to the red point. This means that a

small imaginary frequency term is needed in order to achieve the cancellation of the minimum eigenvalue and, therefore, the cancellation of the determinant of the M matrix. As for the second mode, its complex map shows a minimum shifted to the left part of the map. It can be seen that the minimum is no longer a point but a distributed structure, being this an artifact produced by the discretization of the parameters in the simulation so that an artificial breaking of the degeneracy is found.

By changing the normalized mass of the scatterers, we are able to change their impedance, and then change the behavior of the cluster. Figure 6 left panel shows the evolution of the minimum eigenvalue of the cluster as a function of the twisting angle and the real frequency of the system. This is the same map as in Fig. 5, but this time, the normalized mass is $\gamma_\alpha = 20$. What can be seen from this map is that by reducing the impedance of the scatterers, the behavior at low frequency becomes more complex. Compared to the case $\gamma_\alpha = 200$, this one shows more modes for small angles. Furthermore, dipolar behavior near commensurate angles, which was clear in the previous case whenever $\Omega a/\pi > 1$, is now more confusing. Only when $\Omega a/\pi > 2.5$ dipolar modes appear. Again, two configurations in this map have been chosen, highlighted with red points in the map. Their resonances as a function of the frequency are shown in the upper right panels of Fig. 6. In this case, each resonance is shown in a different graph. We have decided to split it due to the complexity of the curve with frequency. Therefore, the graphs shown are centered in the resonance, not as in Fig. 5, where all the frequency range was plotted. The first resonance, which corresponds to a spatial configuration of $\theta = 8.86°$ and a resonant frequency of $\Omega a/\pi = 3.23$, shows a broad resonance behavior, having a low quality factor ($Q = 5.98$). This result is in accordance with what it is seen in the complex map below. The minimum in the complex map appears shifted with respect to the red point. The imaginary
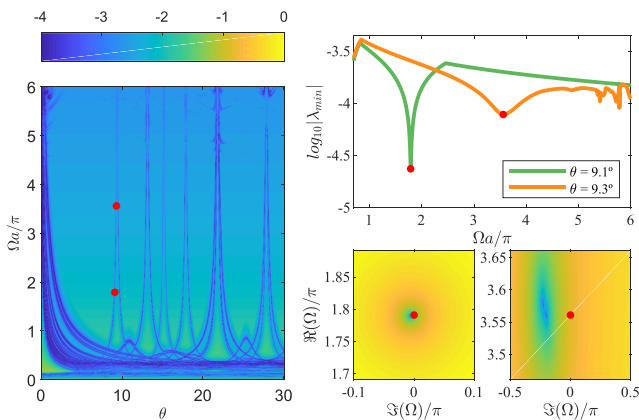

FIG. 5. Left panel: evolution of the minimum eigenvalue of the multiple scattering matrix (M) as a function of the twisting angle of the twisted bilayer structure and the normalized frequency of the system (real frequency). The scatterers' properties are $\gamma_\alpha = 200$ and $\Omega_\alpha \cdot a/\pi = 20$. The original lattices forming the twisted bilayer have a triangular arrangement. Upper right panel: evolution of the minimum eigenvalue as a function of the normalized frequency for two spatial configurations, corresponding to $\theta = 9.1°$ and $\theta = 9.3°$. Lower right panels: these two maps show the evolution of the minimum eigenvalue as a function of the normalized frequency of the system in the complex plane.
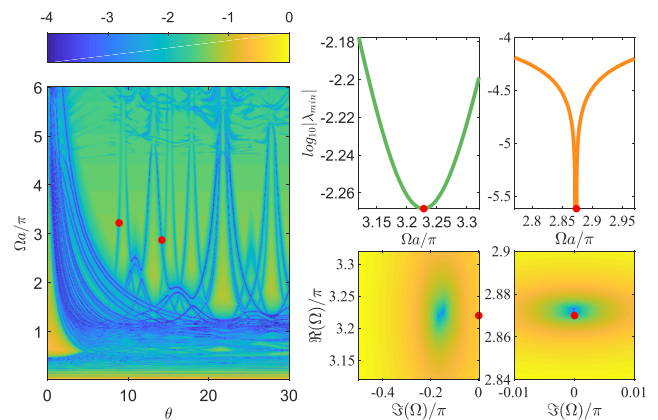

FIG. 6. Left panel: evolution of the minimum eigenvalue of the multiple scattering matrix (M) as a function of the twisting angle of the twisted bilayer structure and the normalized frequency of the system (real frequency). The scatterers' properties are $\gamma_\alpha = 20$ and $\Omega_\alpha \cdot a/\pi = 20$. The original lattices forming the twisted bilayer have a triangular arrangement. Upper right panels: evolution of the minimum eigenvalue as a function of the normalized frequency for two spatial configurations, corresponding to $\theta = 8.86°$ and $\theta = 14.17°$. Lower right panels: these two maps show the evolution of the minimum eigenvalue as a function of the normalized frequency of the system in the complex plane.
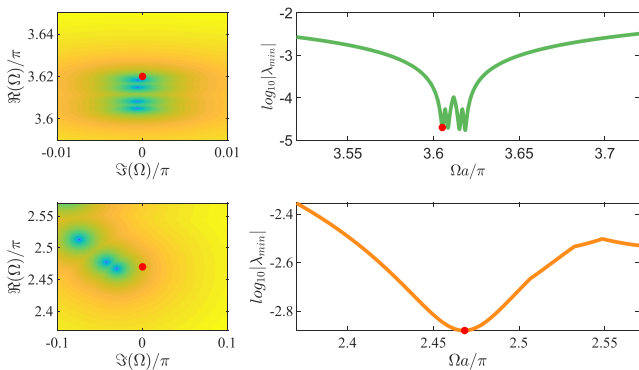
FIG. 7. Two more resonances on the $\gamma_\alpha = 20$ twisted bilayers. The first one ($\theta = 12.47)^\circ$, shown above, has been split in four sharp peaks. The second resonance ($\theta = 0.65)^\circ$, shown below, is a wide one. However, the complex frequency map shows the presence of different minima in the region where the resonance is found.

part needed is higher than in the precedent cases. The second one ($\theta = 14.17^\circ$ and $\Omega a/\pi = 2.88$) shows a sharper behavior, and thus the complex map shows that the minimum is almost at the center of the map, near the brown point. These two cases have similar behavior to those shown for the $\gamma_\alpha = 200$ twisted bilayers.

Finally, other resonances with more complicated behavior can be found in this second structure (twisted bilayers with $\gamma_\alpha = 20$). Figure 7 shows two more resonances (evolution of the minimum eigenvalue with real frequency and the complex frequency map around the resonance point). The one shown in the upper panels has $\theta = 12.47^\circ$ and $\Omega a/\pi = 3.62$, which is located in the dipolar modes of the left panel in Fig. 6. In this case, the resonance is split in four sharp minima. The same behavior is seen in both the real frequency line and the complex map. In the latter, four minima appear with the same imaginary component, which means that the quality factor of these resonances is the same. As for the second mode, the spatial configuration is $\theta = 0.65^\circ$, and the resonant frequency is $\Omega a/\pi = 2.47$. This point belongs to the left part of Fig. 6 left panel, in other words, to the small angle condition, where all the scatterers in the cluster are close to each other. The behavior of the eigenvalue with real frequency shows a single minimum with a wide resonance and a low quality factor ($Q = 20.58$). However, the insight in the complex plane reveals a more complex behavior, with four different minima with different imaginary components and even different real frequencies. As we have found in the aperiodic line of scatterers, this structure also presents some regions with a high density of states.

V. SUMMARY

In summary, we have analyzed the eigenfrequencies of finite clusters of scatters arranged in quasi-periodic distributions by multiple scattering theory. Unlike in previous studies, in which only the position of these modes has been considered, we have focused our study on the quality of these modes, which is a more relevant parameter given the great amount of resonances that these structures present. Two types of clusters have been studied, linear distributions in which the modulation of the distance between scatterers creates

the aperiodicity and twisted bilayers, in which a moiré pattern is formed. The former type of clusters presents localized modes at its edges, although the quality of these modes is remarkably enhanced at the interface between the cluster and its mirror symmetric structure. The latter type of clusters shows as well high quality modes, although a strong variation of this quality can be found through the configuration map, which shows that the analysis of the quality of these modes is more than relevant for their use in operating devices.

AUTHOR DECLARATIONS

Conflict of Interest

The authors have no conflicts to disclose.

Author Contributions

Marc Martí-Sabaté: Conceptualization (equal); Writing – original draft (equal); Writing – review & editing (equal). **Sébastien Guenneau:** Conceptualization (equal); Writing – original draft (equal); Writing – review & editing (equal). **Dani Torrent:** Conceptualization (equal); Writing – original draft (equal); Writing – review & editing (equal).

DATA AVAILABILITY

The data that support the findings of this study are available from the corresponding author upon reasonable request.

REFERENCES

[1] D. Shechtman, I. Blech, D. Gratias, and J. W. Cahn, "Metallic phase with long-range orientational order and no translational symmetry," Phys. Rev. Lett. **53**, 1951–1953 (1984).

[2] L. Bindi, N. Yao, C. Lin, L. S. Hollister, C. L. Andronicos, V. V. Distler, M. P. Eddy, A. Kostin, V. Kryachko, G. J. MacPherson *et al.*, "Natural quasicrystal with decagonal symmetry," Sci. Rep. **5**, 9111 (2015).

[3] X. Cai, L.-J. Lang, S. Chen, and Y. Wang, "Topological superconductor to anderson localization transition in one-dimensional incommensurate lattices," Phys. Rev. Lett. **110**, 176403 (2013).

[4] W. Man, M. Megens, P. J. Steinhardt, and P. M. Chaikin, "Experimental measurement of the photonic properties of icosahedral quasicrystals," Nature **436**, 993–996 (2005).

[5] J.-N. Fuchs and J. Vidal, "Hofstadter butterfly of a quasicrystal," Phys. Rev. B **94**, 205437 (2016).

[6] H. Huang and F. Liu, "Quantum spin hall effect and spin Bott index in a quasicrystal lattice," Phys. Rev. Lett. **121**, 126401 (2018).

[7] J. D. Hays, J. Imbrie, N. J. Shackleton *et al.*, "Variations in the earth's orbit: Pacemaker of the ice ages," Science **194**, 1121 (1976), American Association for the Advancement of Science Washington, DC.

[8] A. Della Villa, S. Enoch, G. Tayeb, V. Pierro, V. Galdi, and F. Capolino, "Band gap formation and multiple scattering in photonic quasicrystals with a Penrose-type lattice," Phys. Rev. Lett. **94**, 183903 (2005).

[9] Y. Cao, V. Fatemi, S. Fang, K. Watanabe, T. Taniguchi, E. Kaxiras, and P. Jarillo-Herrero, "Unconventional superconductivity in magic-angle graphene superlattices," Nature **556**, 43–50 (2018).

[10] H. Polshyn, M. Yankowitz, S. Chen, Y. Zhang, K. Watanabe, T. Taniguchi, C. R. Dean, and A. F. Young, "Large linear-in-temperature resistivity in twisted bilayer graphene," Nat. Phys. **15**, 1011–1016 (2019).

[11] P. Moon and M. Koshino, "Optical absorption in twisted bilayer graphene," Phys. Rev. B **87**, 205404 (2013).

[12] M. I. Rosa, M. Ruzzene, and E. Prodan, "Topological gaps by twisting," Commun. Phys. **4**, 130 (2021).

[13] D. Beli, M. I. N. Rosa, C. De Marqui, Jr. and M. Ruzzene, "Mechanics and dynamics of two-dimensional quasicrystalline composites," Extreme Mech. Lett. **44**, 101220 (2021).

[14] S. M. Kuznetsova, J.-P. Groby, L. M. García-Raffi, and V. Romero-García, "Localized interface modes in one-dimensional hyperuniform acoustic materials," J. Phys. D: Appl. Phys. **54**, 315303 (2021).

[15] Z. V. Vardeny, A. Nahata, and A. Agrawal, "Optics of photonic quasicrystals," Nat. Photonics **7**, 177–187 (2013).

[16] M. A. Bandres, M. C. Rechtsman, and M. Segev, "Topological photonic quasicrystals: Fractal topological spectrum and protected transport," Phys. Rev. X **6**, 011016 (2016).

[17] D. J. Apigo, W. Cheng, K. F. Dobiszewski, E. Prodan, and C. Prodan, "Observation of topological edge modes in a quasiperiodic acoustic waveguide," Phys. Rev. Lett. **122**, 095501 (2019).

[18] X. Ni, K. Chen, M. Weiner, D. J. Apigo, C. Prodan, A. Alu, E. Prodan, and A. B. Khanikaev, "Observation of Hofstadter butterfly and topological edge states in reconfigurable quasi-periodic acoustic crystals," Commun. Phys. **2**, 55 (2019).

[19] M. I. N. Rosa, Y. Guo, and M. Ruzzene, "Exploring topology of 1d quasiperiodic metastructures through modulated LEGO resonators," Appl. Phys. Lett. **118**, 131901 (2021).

[20] R. K. Pal, M. I. N. Rosa, and M. Ruzzene, "Topological bands and localized vibration modes in quasiperiodic beams," New J. Phys. **21**, 093017 (2019).

[21] M. Duneau and A. Katz, "Quasiperiodic patterns," Phys. Rev. Lett. **54**, 2688–2691 (1985).

[22] M. Martí-Sabaté and D. Torrent, "Dipolar localization of waves in twisted phononic crystal plates," Phys. Rev. Appl. **15**, L011001 (2021).

[23] M. Martí-Sabaté and D. Torrent, "Edge modes for flexural waves in quasiperiodic linear arrays of scatterers," APL Mater. **9**, 081107 (2021).

[24] D. Torrent, D. Mayou, and J. Sánchez-Dehesa, "Elastic analog of graphene: Dirac cones and edge states for flexural waves in thin plates," Phys. Rev. B **87**, 115143 (2013).

[25] N. Lera, D. Torrent, P. San-Jose, J. Christensen, and J. V. Alvarez, "Valley Hall phases in Kagome lattices," Phys. Rev. B **99**, 134102 (2019).

[26] A. Karlos, P. Packo, and A. N. Norris, "Nonlinear multiple scattering of flexural waves in elastic beams: Frequency conversion and non-reciprocal effects," J. Sound Vib. **527**, 116859 (2022).

[27] S. Kim and J. E. Pasciak, "The computation of resonances in open systems using a perfectly matched layer," Math. Comput. **78**, 1375–1398 (2009).

[28] X. Ni, K. Chen, M. Weiner, D. J. Apigo, C. Prodan, A. Alù, E. Prodan, and A. B. Khanikaev, "Observation of Hofstadter butterfly and topological edge states in reconfigurable quasi-periodic acoustic crystals," Commun. Phys. **2**(1), 55–61 (2019).

[29] D. R. Hofstadter, "Energy levels and wave functions of Bloch electrons in rational and irrational magnetic fields," Phys. Rev. B **14**, 2239–2249 (1976).

[30] M. Gupta and M. Ruzzene, "Dynamics of quasiperiodic beams," Crystals **10**, 1144 (2020).

[31] C. R. Dean, L. Wang, P. Maher, C. Forsythe, F. Ghahari, Y. Gao, J. Katoch, M. Ishigami, P. Moon, M. Koshino *et al.*, "Hofstadter's butterfly and the fractal quantum Hall effect in moiré superlattices," Nature **497**, 598–602 (2013).